Direct Chemical Vapor Deposition Growth of WS_2 Atomic Layers on Hexagonal Boron Nitride

Mitsuhiro Okada,[†] Takumi Sawazaki,[†] Kenji Watanabe,[‡] Takashi Taniguch,[‡] Hiroki Hibino,[§] Hisanori Shinohara,[†,*] and Ryo Kitaura[†,*]

[†]Department of Chemistry, Nagoya University, Nagoya 464-8602, Japan, [‡]National Institute for Materials Science, 1-1 Namiki, Tsukuba, 305-0044, Japan, and [§]NTT Basic Research Laboratories, NTT Corporation, Atsugi, Kanagawa 243-0198, Japan

ABSTRACT Atomically thin transition metal dichalcogenides (TMDCs) have attracted considerable interest owing to the spin-valley coupled electronic structure and possibility in next-generation devices. Substrates are one of the most important factors to limit physical properties of atomic-layer materials, and among various substrates so far investigated, hexagonal boron nitride (hBN) is the best substrate to explore the intrinsic properties of atomic layers. Here we report direct chemical vapor deposition (CVD) growth of WS_2 onto high-quality hBN using a 3-furnace CVD setup. Triangular-shaped WS_2 grown on hBN have shown limited crystallographic orientation that is related to that of the underlying hBN. Photoluminescence spectra of the WS_2 show an intense emission peak at 2.01 eV with a quite small fwhm of 26 meV. The sharp emission peak indicates the high quality of the present WS_2 atomic layers with high crystallinity and clean interface.

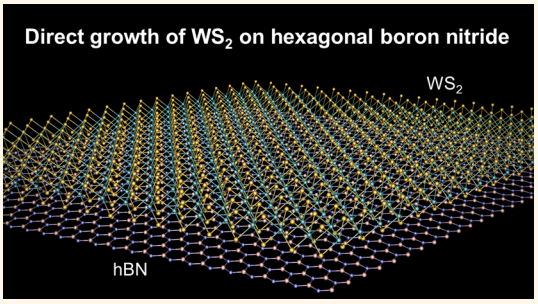

KEYWORDS: transition metal dichalcogenides (TMDCs) · CVD growth · optical properties

Transition metal dichalcogenides (TMDCs) have attracted significant attention in recent years as the emerging postgraphene material.[1−3] Monolayer TMDCs are three-atom-thick sheets, in which remarkable physical properties can be seen owing to their reduced dimensionality.[4] The family of TMDCs, about 40 different known TMDCs with different composition, provides a fundamental and widespread platform to explore optical and electronic properties in two-dimensional systems. Recent studies on TMDCs have shown fascinating properties of TMDCs including the peculiar electronic structure due to spin-valley coupling, strong photoemission in a monolayer of TMDCs, high-performance in field-effect transistors, and application as flexible devices, which indicates a great possibility of TMDCs in next-generation optoelectronics and valleytronics applications.[5−8]

In atomic-layer materials such as graphenes and TMDCs, one of the most crucial factors that limits its physical properties is substrates. Even though carrier mobility of free-standing graphenes exceeds 200 000 $cm^2\ V^{-1}\ s^{-1}$ at 5 K, the typical carrier mobility of high-quality graphene sitting on SiO_2/Si is about 10 000 $cm^2\ V^{-1}\ s^{-1}$.[9−11] This degradation of carrier mobility can be attributed to extrinsic scattering resulting from SiO_2 substrates: charged surface states, charged impurities, substrate roughness, and surface optical phonons.[12] Recent studies have shown that the substrate effect also limits electronic properties of TMDCs, and the substrate effect causes formation of localized states, for example, results in variable range hopping at high temperature and resonant tunneling transport at low temperature.[13]

Hexagonal boron nitride (hBN) has been proven to be the best substrate to observe intrinsic properties of atomic-layer materials.[14] hBN is an insulator with a bandgap of about 6.4 eV and has the identical structure of graphene with boron and nitrogen atoms occupying the A and B sublattices.[15,16] hBN can, therefore, provide an atomically flat surface without dangling bonds and charged impurity: one can mimic the free-standing situation using hBN as substrates. In fact, very high carrier mobility (~60 000 $cm^2\ V^{-1}\ s^{-1}$ at

* Address correspondence to noris@nagoya-u.jp, r.kitaura@nagoya-u.jp.

Received for review May 15, 2014 and accepted August 5, 2014.

Published online August 05, 2014
10.1021/nn503093k

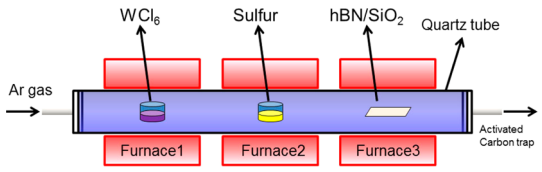

Figure 1. A schematic representation of the 3-furnace CVD apparatus. WCl_6 and sulfur were placed in quartz cups.

room temperature) has been reported on graphenes transferred onto hBN, opening the possibilities of exploring new physics and electronics applications of graphene.[17] TMDCs sitting on hBN are therefore the key structure to explore the intrinsic physical properties of TMDCs such as the photoinduced spin-Hall effect and the valley Hall effect.[5]

We report here a direct CVD growth of TMDCs onto high-quality hBN. Although the TMDC/hBN structure can also be realized by the mechanical-exfoliation-transfer method, the formation of TMDC/hBN by direct CVD growth has great advantages over the transfer method.[18] Because TMDCs are deposited directly onto hBN without any wet-chemical processes by the present direct CVD growth, one can, in principle, realize a clean interface between TMDCs and hBN. In contrast, the transfer method includes a deposition of polymers and a solution-based washing process. The clean interface is one of the key factors to see the intrinsic properties of TMDCs/hBN. In addition, the CVD growth is simple, fast, and scalable. Such merits are essential to facilitate fabrication of TMDCs/hBN devices to explore properties of TMDCs toward realization of next-generation optoelectronic and valleytronics devices.

RESULTS AND DISCUSSION

Our strategy on CVD-growth of TMDCs onto hBN is to use high-quality exfoliated hBN flakes obtained from single-crystal hBN and a newly developed 3-furnace CVD apparatus. Figure 1 shows schematic representation of the 3-furnace CVD setup, which enables us to control independently supply rates of metal source (metal chloride) and chalcogenide and growth temperature; we can control the supply rate by furnace temperature. This independent control of the supply rate and growth temperature is essential so as to stably supply each source with the optimum rate and to thus grow TMDCs at optimum condition. In this CVD growth, tungsten chloride having a low boiling point (611 K under ambient pressure) is used to facilitate the supply of metal source. The hBN flakes used in this study were prepared by mechanical exfoliation from ultrapure single crystals grown by the high-temperature and high-pressure method.[19] Typical size of the exfoliated hBN deposited on SiO_2 is about several tens of micrometers, and the atomically flat surface of the so-prepared hBN was confirmed by AFM observations (the roughness rms is about 0.09 nm, see

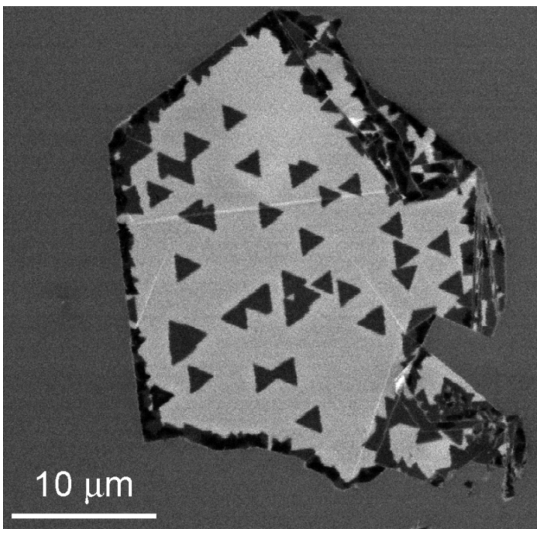

Figure 2. A SEM image of triangular-shaped WS_2 crystals grown onto a hBN flake.

Supporting Information). Raman spectra of the hBN transferred onto SiO_2 shows a sharp Raman band at 1350 cm^{-1} with fwhm (full width at half-maximum) of 9 cm^{-1}, indicating high crystallinity of the exfoliated hBN (see the Raman spectrum in Supporting Information).

Figure 2 shows a SEM image of WS_2 grown directly on hBN (WS_2/hBN) using WCl_6 as a metal source (growth temperature and pressure is 900 K and atmospheric pressure, respectively). As clearly seen in the SEM image, there are strong (dark) triangular contrasts with *ca.* 3 μm average size on hBN, indicating formation of WS_2 crystals with triangular shape. The formation of the triangular-shaped WS_2 can be understood based on the presence of an energetically preferred edge, that is, the zigzag edge.[20,21] The crystal shape is uniquely determined as triangular when the zigzag sulfur edge is assumed. The formation of triangular-shaped WS_2, in fact, has also been observed in previous studies on a CVD growth of TMDCs onto SiO_2.[22−24] As seen in the SEM image, the density of WS_2 crystals at the edge of the hBN flake is much higher than that of the middle part, suggesting that the hBN edge is an effective nucleation site for WS_2 growth. There should be a lot of dangling bonds at the edge of the hBN flakes, and the dangling bonds presumably provide the nucleation site during the growth of WS_2 atomic layers.

Figure 3 shows a Raman spectrum of WS_2/hBN measured with an excitation wavelength of 488 nm. Intense Raman bands centered at 356.3 and 419.4 cm^{-1}, which are respectively assigned to E' and A' Raman active modes, are clearly observed.[25−27] The observed peak positions are different from those of bulk WS_2 (355.5 and 420.5 cm^{-1} for E′ and A′, respectively), and the difference have been attributed to interlayer van der Waals interaction and dielectric screening of the long-range Coulombic interactions between the effective charges. Because the peak shift occurs due to the

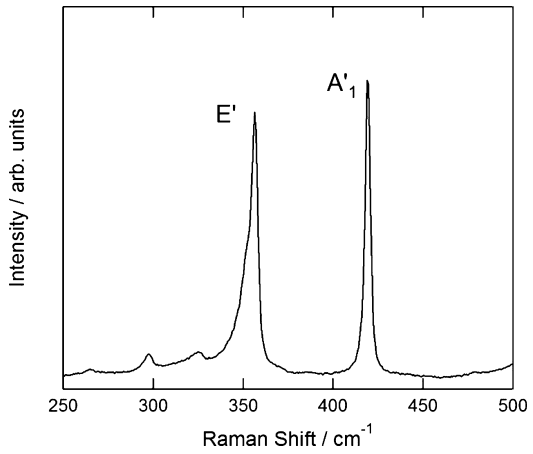

Figure 3. A typical Raman spectrum of WS_2 grown on hBN. The spectrum was measured using excitation wavelength of 488 nm.

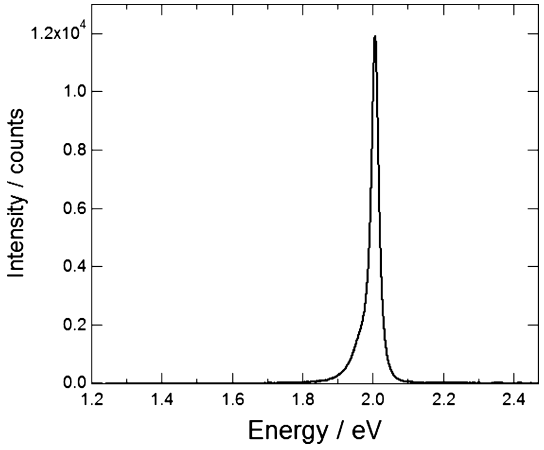

Figure 4. A PL spectrum of WS_2 grown on hBN.

interlayer interaction, the peak position of E' and A' changes depending on the layer number of WS_2; red and blue shifts were observed, respectively, for E' and A' mode when the layer number decreases. The observed peak separation between the E' and A' mode is 62.5 cm^{-1}, which corresponds to the reported peak separation of a single-layer WS_2 on SiO_2 substrates.[23]

Figure 4 shows a photoluminescence (PL) spectrum of WS_2/hBN measured with an excitation wavelength of 488 nm. As seen in the figure, there is a strong peak centered at 2.01 eV. The peak position is comparable to a previously reported value of monolayer WS_2, which is higher than that of multilayer WS_2.[28,29] The fwhm of the PL emission peak is only 26 meV, which is less than half of those previously reported values: 50−55 and 75 meV for CVD-grown and exfoliated WS_2 on SiO_2, respectively.[23,28] Since, in general, the fwhm of PL emission peak is related to exciton lifetime (τ) and interfacial quality, the very small fwhm observed (almost equal to thermal energy at room temperature, 25.8 meV for 300 K) can be attributed to both the high crystallinity of grown WS_2 and the clean interface realized between WS_2 and hBN. One thing should be noted is that the PL peaks observed on WS_2 crystals grown on hBN are much brighter than the peaks of those grown on SiO_2 (Supporting Information), which means that WS_2 grown on SiO_2 are low-quality multilayer flakes. We think that the hBN characteristics, flatness and the fact that no dangling bond exists, play an important role in the formation of high-quality thin WS_2 on hBN.

As seen in Figure 2, the dominant orientation of triangular crystals of WS_2 grown on hBN is limited to two different orientations with a relative angle of 60°. The limited orientation of WS_2 indicates that there is a strict relation in crystallographic orientations between WS_2 crystals and hBN substrates. To investigate the relative orientation in detail, we measured low-energy electron diffraction (LEED) and electron backscattering diffraction (EBSD) patterns of a WS_2/hBN. Figure 5b shows a typical LEED pattern of a WS_2 crystal on hBN. The LEED pattern shows two hexagonal patterns with 3-fold symmetry, which arises from the WS_2 crystal and hBN substrate; note that the strongest hexagonal pattern arises from graphene deposited onto WS_2/hBN to avoid charging. As clearly illustrated, the orientation of the hexagonal lattice of hBN and WS_2 perfectly coincides. In addition, as seen in Figure 5c,d, WS_2 crystals having different orientations of triangular shapes give two different LEED patterns; 60° rotation of one pattern gives the other pattern. This clearly demonstrates that all triangular WS_2 crystals grown on hBN have identical edge structure, which is consistent with the existence of the preferred edge structure. Information on crystal orientation obtained by EBSD is also consistent with the LEED results (Supporting Information). Because of the difference in lattice constants between WS_2 and hBN (the cell parameters a of WS_2 and hBN are 0.318 and 0.250 nm, respectively), WS_2/hBN shows an incommensurate moiré superstructure whose periodicity is about 5 times larger than that of WS_2 (Figure 5e).

The growth mode of WS_2 on hBN would be a Frank-van der Merwe mechanism, where small 2D nuclei are formed and grow to be large 2D crystals. Because WS_2 molecules have no dangling bonds except for edges, additional atoms selectively attach active sites at edges of the nuclei, leading to growth of 2D WS_2 crystals. The question here is why the strict crystallographic relation between WS_2 and hBN appears. The previous studies on CVD-growth of TMDCs on SiO_2 show a random crystallographic orientation of the TMDCs grown on the substrate, and a study on CVD-growth of NbS_2 onto graphene also indicates no strict relation of crystallographic orientation between NbS_2 grown and graphene underneath.[30] One possible explanation is that the growth of WS_2 occurs at step edges of hBN. If this scenario is true, triangle crystals of WS_2 should align in a linear fashion on hBN. This is however inconsistent with most of the observed SEM images (for example,

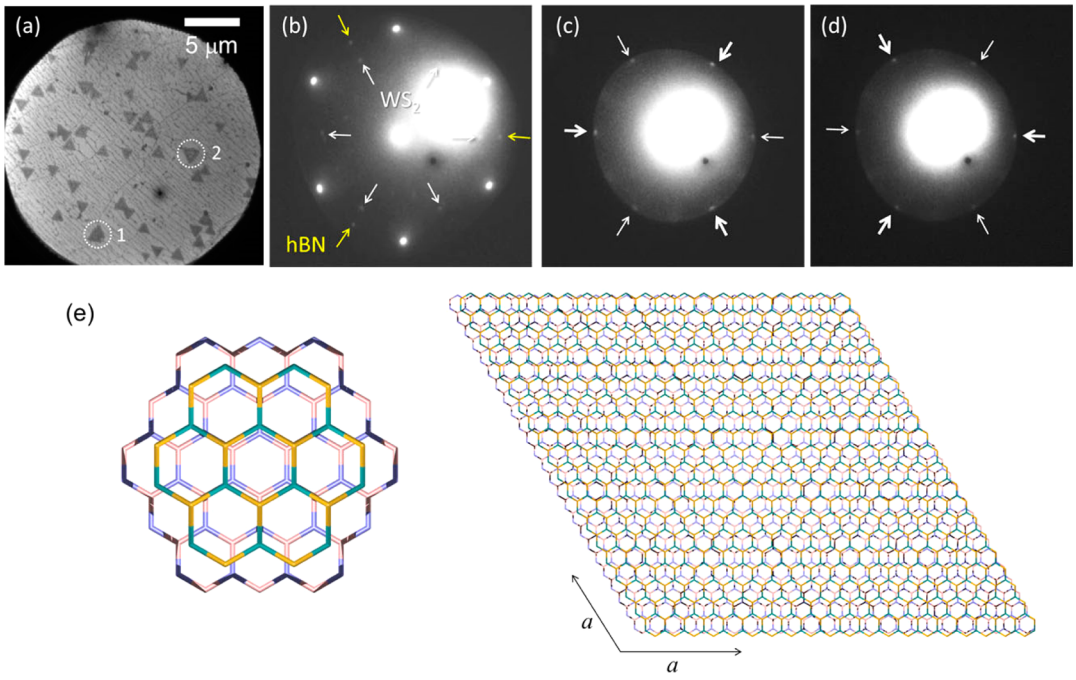

Figure 5. (a) Low-energy electron microscopy image of WS_2 crystal grown on hBN. Images b and c correspond to the LEED patterns measured at position 1 with an electron energy of 50 and 22 eV. Image d corresponds to the LEED pattern measured at position 2 with an electron energy of 22 eV. (e) Proposed structure model of WS_2/hBN constructed on the basis of the SEM image and the EBSD maps; the bottom and top layers correspond to hBN and WS_2, respectively. Pink, light blue, yellow, and green correspond to boron, nitrogen, tungsten, and sulfur atoms, respectively.

Figure 2 and Figure S3 in Supporting Information), and further, AFM observations of exfoliated hBN flakes rarely shows step edges in a flat surface of hBN; a part of Figure S3 shows liner alignment of WS_2 crystals that probably arise from the step-edge initiated growth. The distinct crystallographic relation observed between WS_2 and hBN in the current study thus indicates the presence of substantial interaction between WS_2 and hBN. Because of the difference in electronegativity between B and N, the charge density is polarized toward the N atoms, and the Coulomb interaction, in addition to the van der Waals force, presumably plays a role in determining the orientation of WS_2 on hBN.

On the basis of the above discussion, the proposed growth mechanism is the following. At first, small nuclei of WS_2 form at the hBN (0001) surface. At the early stage of the growth, the small nuclei of WS_2 probably can translate and rotate because there is no direct chemical bond between the nuclei and hBN. As a result of the random motion, nuclei can find energetically favored orientation, leading to the formation of large 2D WS_2 crystals with defined crystallographic orientation. We counted the number of triangular WS_2 crystals in two dominant orientations and found that the two orientations appear equally (Supporting Information), meaning that the energy difference between the two different orientations is small.

CONCLUSIONS

We have newly developed a 3-furnace CVD apparatus and successfully synthesized WS_2 atomic-layers directly onto high-quality hBN. The triangular-shaped WS_2 grown on hBN exhibits Raman bands characteristic to monolayer WS_2 and an intense sharp PL emission peak centered at 2.01 eV. The fwhm of the emission peak is only 26 meV which is much smaller than the previously reported value, indicating that the quality of the present WS_2/hBN sample is extremely high. Furthermore, in contrast to the previous studies on CVD growth of TMDCs, we have observed a distinct crystallographic orientation between the grown WS_2 and hBN, which may arise from the interlayer Coulomb interaction. The present method can be applied to prepare high quality TMDC atomic-layers that are suitable for exploring optical and electronic properties of many other TMDC atomic-layer materials, which promises to initiate a new field based on high-quality TMDCs.

EXPERIMENTAL SECTION

CVD Growth of WS_2. Thin hBN flakes were prepared by mechanical exfoliation. The single crystals of hBN were applied to an adhesive tape, and small thin flakes were prepared by a repeated folding and peeling apart process. The prepared small thin hBN flakes were directly deposited onto Si substrates with SiO_2 film of 100 nm. We synthesized WS_2 on the hBN flakes by

atmospheric pressure CVD using WCl_6 and elemental sulfur as source materials. In brief, 40 mg of WCl_6, 240 mg of elemental sulfur, and a Si substrate with deposited hBN flakes were placed at upper, middle, and the bottom part of a quartz reactor, respectively. We flowed pure Ar (400 sccm), and furnace temperatures at the place where WCl_6 and elemental sulfur were put were set to 353 and 458 K, respectively. The growth of WS_2 was carried out at 1173 K for 10 min. Spectroscopic measurements on products were performed without any post-treatment.

Raman and PL Measurements. Raman and PL spectra were measured using HR-800 (Jovin-Yvon) instrument equipped with solid-state laser operated at 488 nm. A notch filter was used to filter out Rayleigh radiation, and Raman and PL signals were detected with a charge-coupled device (CCD). A 100 × 0.8 NA objective lens was used to focus the laser light on the samples. All measurements were carried out at room temperature and atmospheric conditions.

Conflict of Interest: The authors declare no competing financial interest.

Acknowledgment. This work was supported by Grant-in-aid for Young Scientists A (No. 25708002), Scientific Research on Innovative Areas (No. 25107002), and Scientific Research S (No. 22225001) from MEXT, Japan, and the Global COE Program in Chemistry, Nagoya University.

Supporting Information Available: AFM; Raman spectra of exfoliated hBN; EBSD spectra and mapping; additional images as described in the text. This material is available free of charge via the Internet at http://pubs.acs.org.

REFERENCES AND NOTES

1. Wang, Q. H.; Kalantar-Zadeh, K.; Kis, A.; Coleman, J. N.; Strano, M. S. Electronics and Optoelectronics of Two-Dimensional Transition Metal Dichalcogenides. *Nat. Nanotechnol.* **2012**, *7*, 699–712.
2. Chhowalla, M.; Shin, H. S.; Eda, G.; Li, L. J.; Loh, K. P.; Zhang, H. The Chemistry of Two-Dimensional Layered Transition Metal Dichalcogenide Nanosheets. *Nat. Chem.* **2013**, *5*, 263–275.
3. Huang, X.; Zeng, Z. Y.; Zhang, H. Metal Dichalcogenide Nanosheets: Preparation, Properties and Applications. *Chem. Soc. Rev.* **2013**, *42*, 1934–1946.
4. Mak, K. F.; He, K. L.; Lee, C.; Lee, G. H.; Hone, J.; Heinz, T. F.; Shan, J. Tightly Bound Trions in Monolayer MoS_2. *Nat. Mater.* **2013**, *12*, 207–211.
5. Xiao, D.; Liu, G. B.; Feng, W. X.; Xu, X. D.; Yao, W. Coupled Spin and Valley Physics in Monolayers of MoS_2 and Other Group-VI Dichalcogenides. *Phys. Rev. Lett.* **2012**, *108*, 196802.
6. Eda, G.; Maier, S. A. Two-Dimensional Crystals: Managing Light for Optoelectronics. *ACS Nano* **2013**, *7*, 5660–5665.
7. Mak, K. F.; Lee, C.; Hone, J.; Shan, J.; Heinz, T. F. Atomically Thin MoS_2: A New Direct-Gap Semiconductor. *Phys. Rev. Lett.* **2010**, *105*, 136805.
8. Georgiou, T.; Jalil, R.; Belle, B. D.; Britnell, L.; Gorbachev, R. V.; Morozov, S. V.; Kim, Y. J.; Gholinia, A.; Haigh, S. J.; Makarovsky, O.; *et al*. Vertical Field-Effect Transistor Based on Graphene-WS_2 Heterostructures for Flexible and Transparent Electronics. *Nat. Nanotechnol.* **2013**, *8*, 100–103.
9. Castro, E. V.; Ochoa, H.; Katsnelson, M. I.; Gorbachev, R. V.; Elias, D. C.; Novoselov, K. S.; Geim, A. K.; Guinea, F. Limits on Charge Carrier Mobility in Suspended Graphene Due to Flexural Phonons. *Phys. Rev. Lett.* **2010**, *105*, 266601.
10. Novoselov, K. S.; Geim, A. K.; Morozov, S. V.; Jiang, D.; Zhang, Y.; Dubonos, S. V.; Grigorieva, I. V.; Firsov, A. A. Electric Field Effect in Atomically Thin Carbon Films. *Science* **2004**, *306*, 666–669.
11. Bolotin, K. I.; Sikes, K. J.; Jiang, Z.; Klima, M.; Fudenberg, G.; Hone, J.; Kim, P.; Stormer, H. L. Ultrahigh Electron Mobility in Suspended Graphene. *Solid State Commun.* **2008**, *146*, 351–355.
12. Chen, J. H.; Jang, C.; Xiao, S. D.; Ishigami, M.; Fuhrer, M. S. Intrinsic and Extrinsic Performance Limits of Graphene Devices on SiO_2. *Nat. Nanotechnol.* **2008**, *3*, 206–209.
13. Qiu, H.; Xu, T.; Wang, Z. L.; Ren, W.; Nan, H. Y.; Ni, Z. H.; Chen, Q.; Yuan, S. J.; Miao, F.; Song, F. Q.; et al. Hopping Transport through Defect-Induced Localized States in Molybdenum Disulphide. *Nat. Commun.* **2013**, 3642.
14. Dean, C. R.; Young, A. F.; Cadden-Zimansky, P.; Wang, L.; Ren, H.; Watanabe, K.; Taniguchi, T.; Kim, P.; Hone, J.; Shepard, K. L. Multicomponent Fractional Quantum Hall Effect in Graphene. *Nat. Phys.* **2011**, *7*, 693–696.
15. Watanabe, K.; Taniguchi, T.; Kanda, H. Direct-Bandgap Properties and Evidence for Ultraviolet Lasing of Hexagonal Boron Nitride Single Crystal. *Nat. Mater.* **2004**, *3*, 404–409.
16. Museur, L.; Brasse, G.; Pierret, A.; Maine, S.; Attal-Tretout, B.; Ducastelle, F.; Loiseau, A.; Barjon, J.; Watanabe, K.; Taniguchi, T.; *et al*. Exciton Optical Transitions in a Hexagonal Boron Nitride Single Crystal. *Phys. Status Solidi-R* **2011**, *5*, 214–216.
17. Dean, C. R.; Young, A. F.; Meric, I.; Lee, C.; Wang, L.; Sorgenfrei, S.; Watanabe, K.; Taniguchi, T.; Kim, P.; Shepard, K. L.; *et al*. Boron Nitride Substrates for High-Quality Graphene Electronics. *Nat. Nanotechnol.* **2010**, *5*, 722–726.
18. Lee, G. H.; Yu, Y. J.; Cui, X.; Petrone, N.; Lee, C. H.; Choi, M. S.; Lee, D. Y.; Lee, C.; Yoo, W. J.; Watanabe, K.; *et al*. Flexible and Transparent MoS_2 Field-Effect Transistors on Hexagonal Boron Nitride–Graphene Heterostructures. *ACS Nano* **2013**, *7*, 7931–7936.
19. Taniguchi, T.; Watanabe, K. Synthesis of High-Purity Boron Nitride Single Crystals under High Pressure by Using Ba–BN Solvent. *J. Cryst. Growth* **2007**, *303*, 525–529.
20. van der Zande, A. M.; Huang, P. Y.; Chenet, D. A.; Berkelbach, T. C.; You, Y. M.; Lee, G. H.; Heinz, T. F.; Reichman, D. R.; Muller, D. A.; Hone, J. C. Grains and Grain Boundaries in Highly Crystalline Monolayer Molybdenum Disulphide. *Nat. Mater.* **2013**, *12*, 554–561.
21. Najmaei, S.; Liu, Z.; Zhou, W.; Zou, X. L.; Shi, G.; Lei, S. D.; Yakobson, B. I.; Idrobo, J. C.; Ajayan, P. M.; Lou, J. Vapour Phase Growth and Grain Boundary Structure of Molybdenum Disulphide Atomic Layers. *Nat. Mater.* **2013**, *12*, 754–759.
22. Ji, Q. Q.; Zhang, Y. F.; Gao, T.; Zhang, Y.; Ma, D. L.; Liu, M. X.; Chen, Y. B.; Qiao, X. F.; Tan, P. H.; Kan, M.; *et al*. Epitaxial Monolayer MoS_2 on Mica with Novel Photoluminescence. *Nano Lett.* **2013**, *13*, 3870–3877.
23. Gutierrez, H. R.; Perea-Lopez, N.; Elias, A. L.; Berkdemir, A.; Wang, B.; Lv, R.; Lopez-Urias, F.; Crespi, V. H.; Terrones, H.; Terrones, M. Extraordinary Room-Temperature Photoluminescence in Triangular WS_2 Monolayers. *Nano Lett.* **2013**, *13*, 3447–3454.
24. Xu, K.; Wang, Z. X.; Du, X. L.; Safdar, M.; Jiang, C.; He, J. Atomic-Layer Triangular WSe_2 Sheets: Synthesis and Layer-Dependent Photoluminescence Property. *Nanotechnology* **2013**, *24*, 465705.
25. Zeng, H. L.; Liu, G. B.; Dai, J. F.; Yan, Y. J.; Zhu, B. R.; He, R. C.; Xie, L.; Xu, S. J.; Chen, X. H.; Yao, W.; *et al*. Optical Signature of Symmetry Variations and Spin-Valley Coupling in Atomically Thin Tungsten Dichalcogenides. *Sci. Rep.* **2013**, *3*, 1608.
26. Elias, A. L.; Perea-Lopez, N.; Castro-Beltran, A.; Berkdemir, A.; Lv, R. T.; Feng, S. M.; Long, A. D.; Hayashi, T.; Kim, Y. A.; Endo, M.; *et al*. Controlled Synthesis and Transfer of Large-Area WS_2 Sheets: From Single Layer to Few Layers. *ACS Nano* **2013**, *7*, 5235–5242.
27. Terrones, H.; Del Corro, E.; Feng, S.; Poumirol, J. M.; Rhodes, D.; Smirnov, D.; Pradhan, N. R.; Lin, Z.; Nguyen, M. A. T.; Elias, A. L.; *et al*. New First Order Raman-active Modes in Few Layered Transition Metal Dichalcogenides. *Sci. Rep.* **2014**, *4*, 4215.
28. Zhao, W. J.; Ghorannevis, Z.; Chu, L. Q.; Toh, M. L.; Kloc, C.; Tan, P. H.; Eda, G. Evolution of Electronic Structure in Atomically Thin Sheets of WS_2 and WSe_2. *ACS Nano* **2013**, *7*, 791–797.
29. Zhao, W. J.; Ribeiro, R. M.; Toh, M. L.; Carvalho, A.; Kloc, C.; Neto, A. H. C.; Eda, G. Origin of Indirect Optical Transitions in Few-Layer MoS_2, WS_2, and WSe_2. *Nano Lett.* **2013**, *13*, 5627–5634.
30. Ge, W. Y.; Kawahara, K.; Tsuji, M.; Ago, H. Large-Scale Synthesis of NbS_2 Nanosheets with Controlled Orientation on Graphene by Ambient Pressure CVD. *Nanoscale* **2013**, *5*, 5773–5778.